15th IFK
Proc. of the 15th International Fluid Power Conference <Symposium/Conference>
<DOI>

Hydraulic Spool Valve Contamination Susceptibility Test and Visualization Study of Clearance Particle Ingress-Aggregation Phenomenon

Chen Qianpeng, Ji Hong, Xie Huan, Ding Ling

School of Energy and Power Engineering, Lanzhou University of Technology, Lanzhou, 730050, China

Key Laboratory of Special Pumps, Valves and Flow Control Systems, Ministry of Education, Lanzhou 730050, China

chenqianpenglut@163.com

Abstract.

During hydraulic equipment service, solid particles infiltrate the oil due to component wear or external contamination, leading to oil contamination. The ingress of contaminated particles into spool valve clearances can cause abrupt increases in spool friction force, resulting in control valve malfunctions and even catastrophic hydraulic system failures. This study focuses on a threaded cartridge directional valve, constructing a contamination susceptibility test rig to investigate the effects of particles with varying contamination levels (10-300 mg/L) and size ranges (0-3 μm, 0-5 μm, 0-10 μm, 0-20 μm, 0-30 μm) on spool friction. It was found that for a unilateral clearance of 5-10 μm, "sensitive particles" (0-10 μm, comparable to the clearance size) induced the maximum electromagnetic driving force on the spool, reaching 150.5 N at 200 mg/L—5 times greater than in clean oil. To unveil the microscopic mechanism of friction escalation caused by sensitive particles, a visualized model experiment was designed, capturing the complete process of particle ingress and aggregation within the clearance using high-speed cameras. Finally, the particle ingress rate in the clearance was calculated via the Discrete Phase Model (DPM), and three optimized structures were proposed based on visualization and simulation results, reducing particle ingress by 80% and mitigating spool sticking risks. This study elucidates the macro-phenomena and micro-mechanisms of "sensitive particle"-induced spool sticking while providing improvement strategies, offering experimental methodologies and theoretical foundations for high-reliability hydraulic spool valve design and contamination control.

Keywords. hydraulic spool valve, friction force, sensitive particles, visualization, structural improvements.

1. INTRODUCTION

Cartridge valves are widely used in hydraulic control systems of engineering machinery and marine equipment due to their compact structure and ease of installation [1]. Among them, spool-type cartridge valves employ high-precision spools with a typical unilateral clearance of 5–10 μm, which provides sealing and guidance functions. As a typical configuration of control valves, the spool features a long cylindrical shaft structure that regulates the flow direction and throttling area of the fluid, thereby determining key parameters such as flow rate and pressure[2-5]. Under high temperature, high pressure, and heavily contaminated conditions, the spool is susceptible to sticking caused by multiphysics coupling effects, which severely compromises control accuracy and response performance[6-9]. Therefore, conducting experimental studies on contaminant-induced jamming and visualizing particle migration and accumulation in spool valves will contribute to improving the theoretical framework of spool design.

Research indicates that spool valve sticking is primarily caused by radial unbalanced forces, non-uniform thermal deformation, and particle intrusion into the clearance. Lin et al. systematically analyzed the mechanisms of these three factors and proposed corresponding suppression strategies; their numerical study based on a solid-liquid two-phase flow model further revealed the migration and sticking patterns of particles within the clearance[10, 11]. Qian et al. found that particles tend to accumulate in the pressure balancing groove regions, and the groove geometry affects the magnitude of the sticking force[12]. Among different groove shapes, the triangular groove demonstrated the best anti-sticking performance due to its minimal fluid deflection and the tendency for particles to settle at the bottom of the groove. Brazhenk experimentally determined the influence of particle size and concentration on the sticking and wear of hydraulic valves, noting that aerospace hydraulic valves are particularly sensitive to certain particle sizes[13]. Furthermore, numerous scholars have experimentally and numerically investigated particle migration, retention, dynamics, and force characteristics in fluid media[14-17].

In terms of visualization studies, Jianjun Zhang et al. employed fluid-structure interaction simulations and high-speed photography of enlarged models to reveal the dynamic process of micron-sized particles entering the clearance, validating the effectiveness of the numerical approach[18]. Xinqiang Liu et al. conducted microscopic observation and simulation analysis to systematically investigate particle trajectories and erosion characteristics at the throttle orifice of servo valves, clarifying the influence of pressure difference, particle shape, and size on erosion behavior. These studies provide important insights for understanding the microscopic movement mechanisms of particles and for structural optimization [19][20].

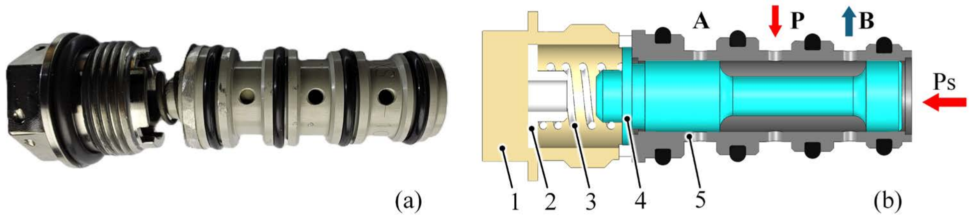

1 screw cap; 2 spring seat; 3 spring; 4 valve spool;5 valve sleeve

(a) Physical diagram of the spool-type directional control valve (b) 3D Structural diagram of the spool-type directional control valve

Figure 1.1. Physical and Three-Dimensional Structural Diagrams of the Spool-Type Directional Control Valve

The studied object is a spool-type directional valve used to regulate hydraulic circuits in a hydraulic system. Its structure and operating principle are shown in Figure. 1.1. The valve consists of a screw cover, spring seat, spring, sleeve, and spool. It is a two-position, three-way valve with a pressure inlet (P) and two outlet ports (A and B). When the actuation force (Ps) is not applied, the spool remains in the right position due to the spring force, connecting P to B. When Ps is applied, the spool moves to the left against the spring force, thereby connecting P to A.

2. Measurement of Contamination-Induced Friction Force in Spool-Type Directional Control Valves

2.1. Design of the Experimental Plan

2.1.1. Test Principle, Working Medium, and Selection of Critical Components

Figure 2.1 shows the schematic diagram of the component contamination susceptibility test. Pressure and flow rate can be adjusted by controlling the throttle valve and the electric motor. A switching mechanism between the contaminated oil tank and the clean oil tank is adopted: the contaminated tank is used to evaluate the external characteristics of the valve under working media of different contamination levels, while the clean tank serves to flush out solid particles remaining in the system, thereby facilitating subsequent test cycles. A water-cooled oil cooler is employed to provide forced heat exchange, dissipating heat generated during system operation and minimizing the impact of temperature on the experimental results.

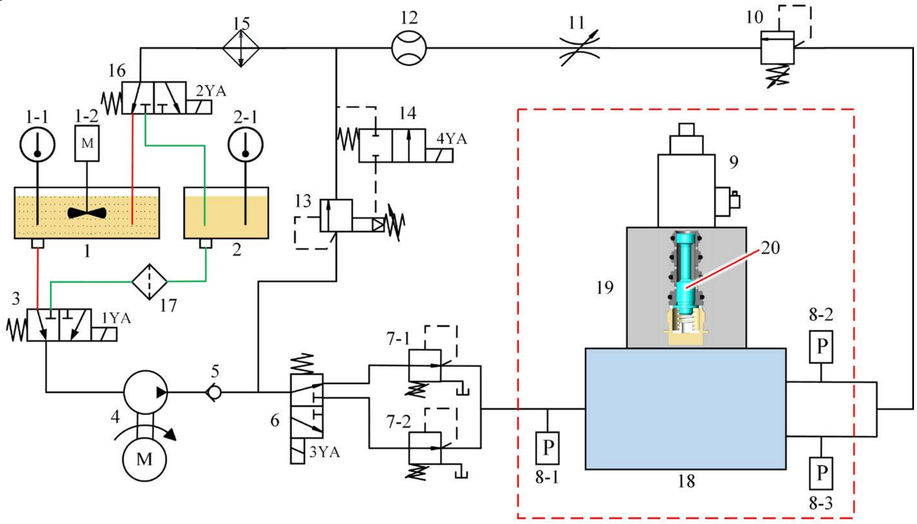

1 Contaminate oil tank; 2 Clean oil tank; 1-1, 2-1Temperature sensor; 1-2 Particle agitator; 3,6,16 Two-position three-port directional control valve; 4 Motor-pump unit; 5 Check valve; 7-1,7-2 Fixed pressure reducing valve; 8-1, 8-2, 8-3, Pressure sensor; 9 Proportional solenoid + displacement sensor (PM + LVDT); 10 Relief valve; 11 Adjustable throttle valve; 12 Flow meter; 13 Safety valve; 14 Unloading valve; 15 Cooler; 17 Filter; 18 Base manifold; 19 Test manifold; 20 Test valve

Figure 2.1. Schematic diagram of the external characteristic test for contamination sensitivity

For other key components in the system, such as the hydraulic pump, an Italian HAWK high-pressure piston pump, model NHD1525L, was employed. This pump features ceramic pistons, which offer high hardness and strong contamination resistance. Its inlet filtration accuracy is 150 μm, allowing it to accommodate the particle sizes introduced in the experiments. The high contamination resistance makes it suitable for contamination susceptibility tests on this platform, as the addition of particles to the working fluid has minimal impact on the pump's performance and does not affect the final test results of the valve. To further minimize the influence of particles introduced into the system during experiments, all tubing and valve components were made of stainless steel.

Given the physical properties of aviation kerosene at 20°C – density range 775–830 kg/m³ and kinematic viscosity 1.25 mm²/s – an ethylene glycol aqueous solution was formulated to match these characteristics. Experimental curve fitting of kinematic viscosity versus glycol concentration at 20°C (Figure 2.2) revealed that an 11.37% ethylene glycol solution by mass exhibits the closest match to the kerosene's properties. Consequently, this 11.37% concentration was ultimately selected as the working fluid substitute.

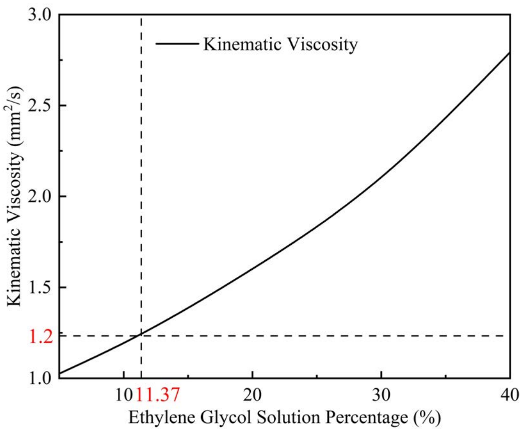

Figure 2.2. Kinematic Viscosity of Ethylene Glycol Aqueous Solutions at Varying Concentrations

2.2. Test Bench Construction and Experimental Results Analysis

2.2.1. Test Bench Construction

The test bench model is shown in Figure. 2.3(a). It features an integral frame structure with a triple-compartment tank arranged on the right side. From back to front, these are the contaminated oil tank, the clean oil inlet tank, and the clean oil return tank. The contaminated oil tank is equipped with an agitator operating at 60–200 r/min, suitable for mixing low-viscosity fluids. The agitator shaft and impeller are made of 304 stainless steel, and a thermocouple is installed in the tank to monitor the oil temperature in real time. Components such as the cooler, agitator, and manual directional valve are mounted on top of the tank. The operating panel is equipped with an adjustable shut-off valve, two pressure-reducing valves, pressure gauges, and a paperless recorder. The test valve block is placed separately on the left side for easy disassembly and installation. The lower cabinet contains the electric motor, frequency converter, flow meter, and solenoid directional valve. To measure the friction force during the movement of the spool in the directional valve, a proportional solenoid with a rated stroke of 8 mm was selected. Within its rated stroke range, the thrust force is proportional to the current supplied to its coil. The stroke-force characteristic curve of the solenoid is shown in Figure. 2.3(b). Within the rated stroke range, the variation in stroke has almost no effect on the force.

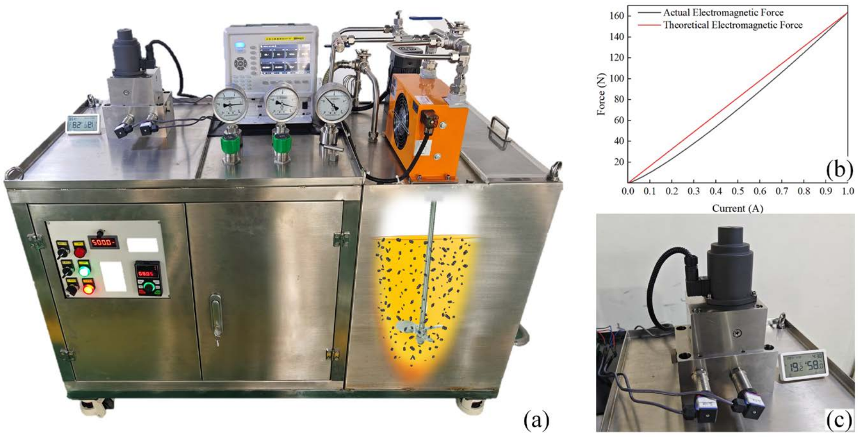

(a) Test Bench Model; (b) Solenoid Current-Force Characteristic Curve; (c) Physical Views of the Base and Test Manifolds

Figure 2.3. Test Bench Model and Physical Views of the Base and Test Manifolds

2.3. Analysis of Experimental Results

The experiment maintained an inlet pressure of 2 MPa and an outlet pressure slightly below 2 MPa, with a flow rate of 3–4 L/min. The directional valve spring preload was set to 22.4 N. After 3 minutes of continuous operation, force was gradually applied to the right end of the valve spool via the solenoid. Pressure transients in both outlet branches were monitored while solenoid current values were recorded to indirectly determine the stiction force magnitude. To investigate variations in the valve's external characteristics under contamination, particle size ranges were selected: 0~3 μm, 0~5 μm, 0~10 μm, 0~20 μm, and 0~30 μm. To prevent frequent spool seizure from high initial concentrations, particle concentration was incrementally increased from 10 mg/L to 300 mg/L in 10 mg/L steps. For each particle size, 31 distinct concentration levels were tested. Stiction force was measured every 3 minutes per condition, with four consecutive measurements averaged per data point.

As shown in Figure 2.4, the line plots illustrate variations in solenoid thrust force under different particle sizes and concentrations. Initially, the solenoid thrust force in particle-free working medium was 26.6 N. For particle sizes of 0~3 μm, the maximum solenoid thrust force reached 73.54 N; for 0~5 μm particles, it increased to 79.63 N; and for 0~10 μm particles, the thrust force surged to 127.7 N. A pronounced stiction phenomenon was observed with rising particle concentrations. Notably, once the concentration exceeded 300 mg/L, the solenoid-driven spool movement could not be reset by the spring force after actuation. For 0~20 μm particles, the maximum solenoid thrust force decreased to 84.73 N, representing a 33.6% reduction compared to the 0~10 μm particle case. With 0~30 μm particles, the maximum thrust force further dropped to 62.14 N, and no stiction occurred during testing. These results indicate that 0~10 μm particles act as critical particles (sensitive particles) in this system. Particles smaller than 0~10 μm are flushed out of the spool valve clearances by the fluid medium, while larger particles (exceeding 0~10 μm) cannot enter the narrow clearances, thereby failing to generate significant stiction forces. 0~10μm particles caused larger thrust fluctuations, while other sizes also caused fluctuations but with smaller amplitude than 0-10μm particles.

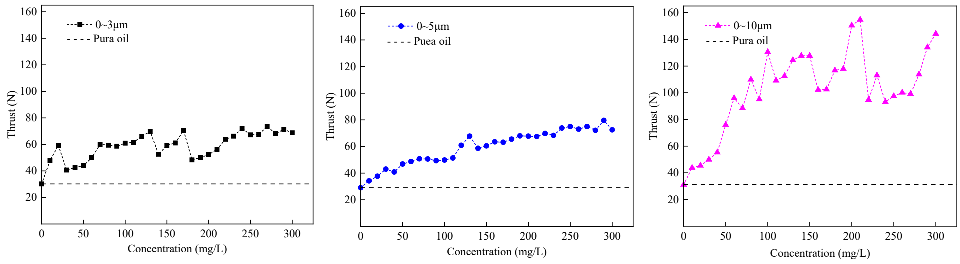

(a) Particle Size: 0~3 μm (b) Particle Size: 0~5 μm (c) Particle Size: 0~10 μm

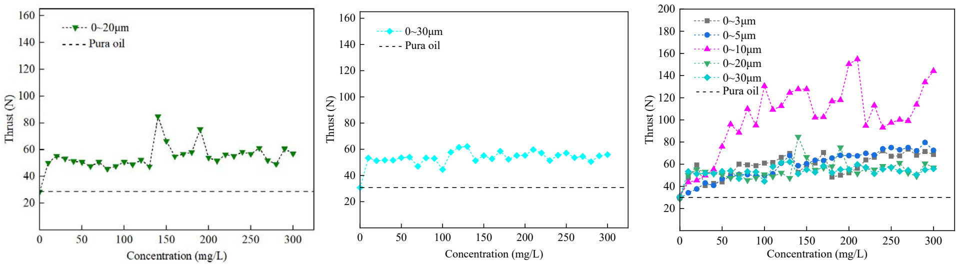

(d) Particle Size: 0~20 μm (e) Particle Size: 0~30 μm (f) Solenoid Thrust Force Variation with Particle Size and Concentration

Figure 2.4. Line Plots of Solenoid Thrust Force Variation with Particle Size and Concentration

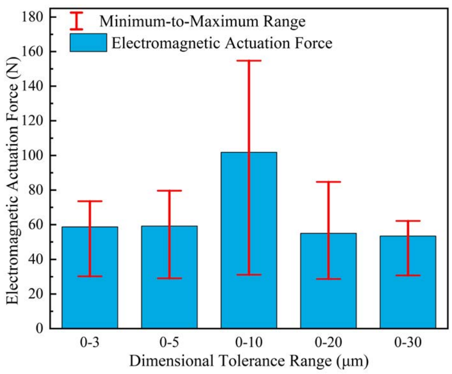

Figure 2.5. the maximum, minimum, and average solenoid forces under different particle sizes

As shown in Figure 2.5, the maximum, minimum, and average solenoid forces under different particle sizes are presented. The stiction force increases with particle size until the particle size exceeds the spool valve clearances, beyond which the stiction force diminishes accordingly.

As shown in Figure 2.6, during spool valve operation, solid particles smaller than the valve mating clearance enter the clearance with the fluid medium. A portion of these particles exit with the fluid flow, while others remain trapped within the clearance. Over time, particles gradually accumulate in the clearance. For an individual particle, when its upper and lower surfaces simultaneously contact the spool and valve body, the particle rotates under torque due to spool movement. To further investigate particle retention within valve clearances, subsequent sections present simulation and experimental visualization studies of particle ingress dynamics.

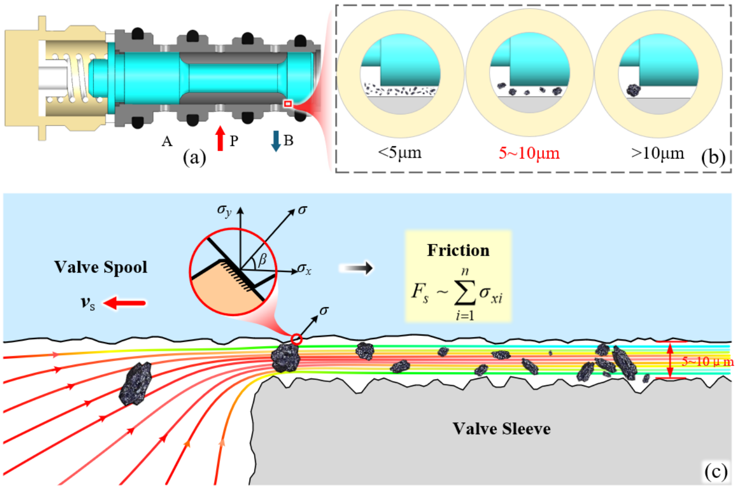

Figure 2.6. Schematic of Particle Invasion into Clearances

3. VISUALIZATION STUDY OF PARTICLE INVASION INTO CLEARANCES

3.1. *Flow Field Simulation and Results Analysis*

3.1.1. *Simulation Model and Parameter Settings*

Given the substantial number of particles invading the clearance and the requirement for computational efficiency, the three-dimensional spool valve model with clearances was simplified to a two-dimensional model, with simulations conducted exclusively for the P-B operating condition (P port connected to B port). The spool-sleeve clearance range of 5~10 μm was represented by a 10 μm clearance in the simulation model. Local mesh refinement ensured grid skewness below 0.6, yielding a final mesh of 500,000 cells; the partitioned fluid domain mesh is illustrated in Figure 3.1 (a).

The fluid phase is fuel, with boundary conditions set as a pressure inlet (1 MPa) and pressure outlet (0 MPa). Three outlets were defined in the simulation: two clearance outlets and one main flow path outlet. For the particle phase, iron particles were selected for trajectory tracking, capturing their motion from injection to escape from the valve chamber fluid domain. Three particle sizes were tested: 5 μm, 8 μm, and 10 μm. Particles were injected from the inlet surface with incident directions spanning an angular range of 30° to 150°. Each simulation cycle injected 10 particles of each size (30 particles per cycle), repeated for 20 cycles (totaling 600 particles). The inlet and outlet boundaries were defined as escape boundaries, while the walls were set as rebound boundaries. Figure 3.1(b) displays flow streamlines within the valve chamber, revealing distinct vortices in the upper and lower regions where particles become entrained in rotational motion.

Figure 3.1(c) illustrates the particle trajectory diagram. A minority of particles follow Path 1 into the upper chamber, while most migrate downward via Path 2. Particles along Path 2-1 flow directly to the outlet, whereas those on Path 2-2 collide with the wall. Post-collision, some particles invade the lower clearance via Path 3, while others enter Path 4, entrained in the vortex flow. Vortex-driven particles either escape through the outlet or invade the lower clearance. Over time, more particles accumulate in the lower clearance than in the upper clearance, with numerous particles circulating persistently in the lower vortex.

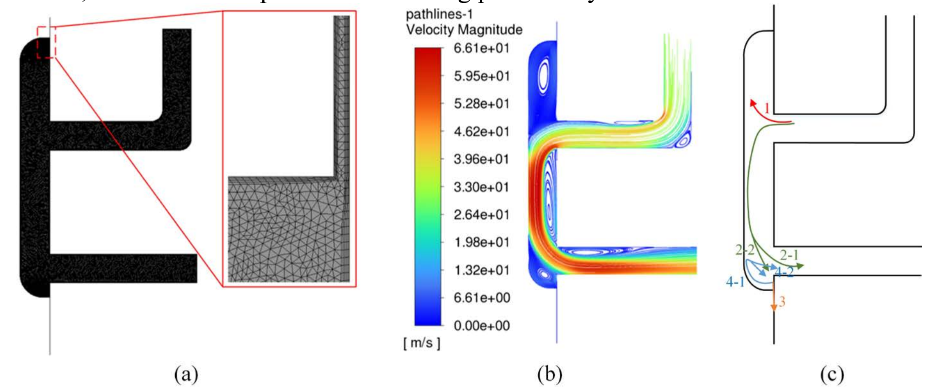

(a) Simulation Model Mesh Generation; (b) Flow Trace Diagram; (c) Particle Trajectory Diagram
Figure 3.1. 2D Simulation Model and Mesh Generation

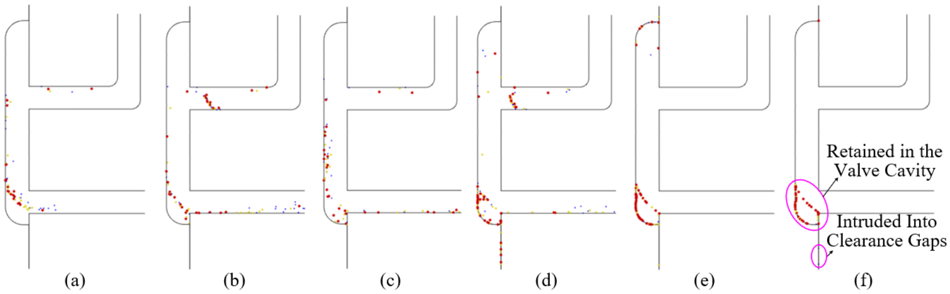

Figure 3.2. Particle Position Diagrams at Different Time Instants

Figure 3.2 depicts particle positions in the valve chamber at different simulation stages. For clarity, particles are magnified 30 times. Blue, yellow, and red represent 5 μm, 8 μm, and 10 μm particles, respectively. Initially, particles are dispersed randomly. As the simulation progresses, their migration patterns align with flow dynamics. In later stages, 34 particles remain trapped in the chamber, rotating along the lower vortex traces.

3.1.2. Particle Migration and Invasion Analysis

The particle retention rate (mechanical trapping ratio) is defined as the ratio of particles remaining in the valve chamber at the end of the simulation to the total injected particles, while the invasion rate represents the ratio of particles invading the clearances to the total injected particles. For the P-B operating condition, the particle retention rate in the valve chamber was 34/600 = 5.6%, with a total invasion rate of 35/600 = 5.9%. Specifically, the invasion rate into the lower clearance was 22/600 = 3.7%, and into the upper clearance was 13/600 = 2.2%. The retention and invasion rates are summarized in Figure 3.3.

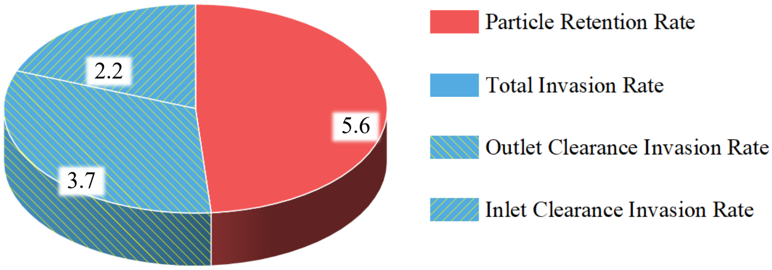

Figure 3.3. Retention and Invasion Rates of Particles in the Valve Chamber

3.2. *Experimental Model Design*

To investigate particle invasion dynamics within valve clearances, the 3D spool valve chamber was simplified to a 2D planar model. Flow channels were machined into an aluminum alloy plate with a uniform groove depth of 0.6 mm. Given the practical impossibility of directly observing sub-micron particle motion within the actual 5~10 μm spool-sleeve clearance and manufacturing constraints for experimental models at this scale, the clearance was geometrically scaled up by 10× to 0.1 mm (100 μm), with contaminant particles proportionally enlarged to 70~120 μm. Figures 3.4(a) and (b) show the 3D spool valve configuration and its corresponding 2D planar flow channel equivalent.

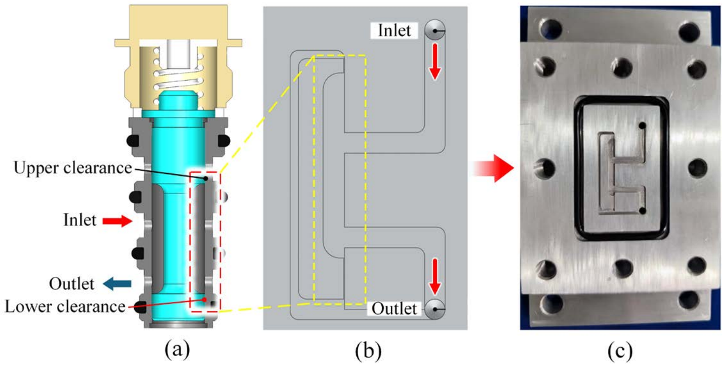

(a) 3D Directional Control Valve Model; (b) Simplified Experimental Model Schematic; (c) Physical Assembly of the Experimental Model

Figure 3.4. 3D Valve Model, Simplified Experimental Model, and Experimental Assembly

The 2D visualization setup comprises two layers: Lower layer: Aluminum alloy base plate featuring machined flow channels and perimeter sealing grooves, with side-mounted threaded ports for fluid connections. The clearance outlet connects to the flow channel at the end of the plate. Upper layer: A transparent acrylic plate for real-time observation of particle motion. The two layers are sealed using a rubber sealing gasket and fastened with bolted connections. The assembled experimental model is illustrated in Figure 3.4(c).

3.3. *Test Bench Design*

Considering the hazardous nature of fuel and the need for high imaging clarity, a water-based medium with comparable density and viscosity was selected as the working fluid. The schematic of the visualization system is shown in Figure 3.5(a). The experimental setup consists of a hydraulic water system and a high-speed camera system. A constant pressure is supplied to the system by an elevated water tank 3. The water pump 2 draws fluid from the supply tank 1 to feed the elevated tank 3. The outlet of the elevated tank 3 is connected to the test model 7 via a pipeline with a shut-off valve 4. Contaminant iron particles are injected into the flow upstream of the test model 7 using a particle injector 6. The fluid then returns to the return water tank 10. During high-speed camera recording, lighting 5 illuminates the test section. The motion of particles within the flow field of the test model 7 is captured by the high-speed camera 9 and transmitted to the computer 8 for analysis.

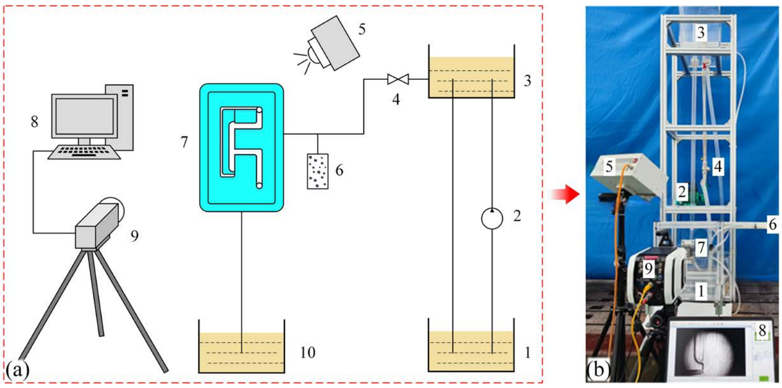

1 Supply water tank; 2 Water pump; 3Elevated water tank; 4 Shut-off valve; 5 Light source;
6 Particle injector; 7 Test model; 8 Computer; 9 High-speed camera; 10 Return water tank
(a) Schematic of the Visualization Test System; (b) Physical View of the Visualization Test System

Figure 3.5. Schematic and Physical View of the Visualization Test System

As shown in Figure 3.5(b), the physical experimental system is displayed. The test frame is constructed entirely from aluminum alloy profiles. Both the low-level and high-level water tanks are fabricated as bonded assemblies of transparent acrylic panels, enabling real-time monitoring of water levels. The 1.6 m height difference between the water level and the manifold inlet corresponds to an inlet pressure of 15.68 kPa (calculated via hydrostatic pressure: $\mathrm{P}=\rho\mathrm{gh}P=\rho gh$).

3.4. Analysis of Experimental Results

During testing, the two clearance regions of the spool valve were primarily imaged to observe particle invasion into the clearances. Since post-shutdown particle accumulation is a critical factor in spool stiction, particle deposition within the valve chamber and clearances was recorded 5 minutes after system shutdown. The high-speed camera captured 10,000 frames per second (fps), with a maximum recording duration of 3 seconds per session. To focus on critical dynamics, the motion trajectories of select particles within the valve chamber and invading the clearances were selectively recorded. Due to the camera's limited field of view, imaging was divided into the upper and lower valve chamber regions.

Figure 3.6(a)(b) shows the 3D schematic of the spool valve and the imaged upper chamber and upper clearance. Three primary particle trajectories are marked: Path 1: Particles migrating toward the outlet. Path 2: Particles invading the clearance. Path 3: Particles colliding with the wall and subsequently flowing toward the outlet. The majority of particles follow Path 1 toward the outlet, while a portion of particles collide with the wall along Path

2, either invading the upper clearance or moving along the wall surface. Another subset of particles collides with the upper spool wall along Path 3 before redirecting toward the outlet.

Figure 3.6(a)(c) shows the 3D schematic of the spool valve and the imaged lower chamber and lower clearance. Three primary particle trajectories are marked: Path 1: Particles migrating toward the outlet. Path 2: Particles invading the clearance. Path 3: Particles colliding with the wall, rotating within the chamber, and subsequently flowing toward the outlet. The majority of particles follow Path 1 toward the outlet. A subset collides with the wall along Path 2 and invades the clearance, while others collide with the wall along Path 3 before redirecting to the outlet.

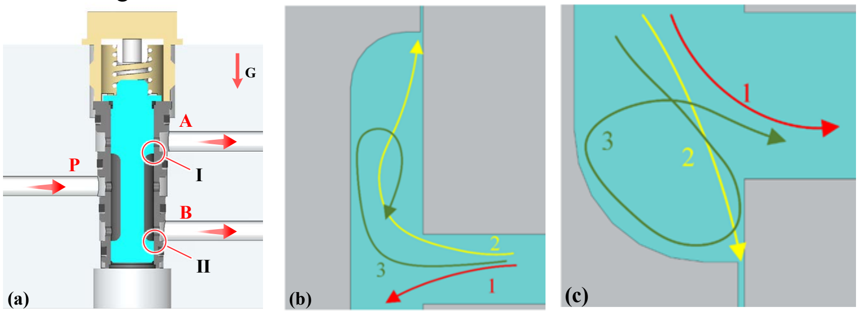

(a) Upper and Lower Valve Chamber (b) I: Particle Trajectory Diagram
(c) II: Particle Trajectory Diagram
(G: Direction of gravity, I: Capture images of the upper valve chamber and upper clearance region, II: Capture images of the lower valve chamber and lower clearance region)
Figure 3.6. Upper and Lower Valve Chamber Section and Marked Particle Trajectories

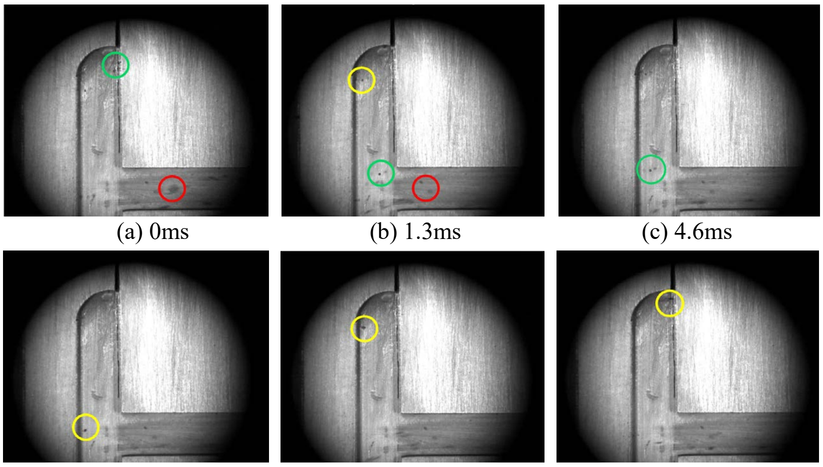

(a) 0ms (b) 1.3ms (c) 4.6ms
(d) 22.2ms (e) 26.2ms (f) 33.8ms
Figure 3.7. Particle Positions in the Upper Valve Chamber at Different Time Instants

Figure 3.7 illustrates the particle positions in the upper valve chamber at different time instants. Key observations include: Particles along Path 1 exhibit significantly higher velocities as they flow toward the outlet. Particles along Paths 2 and 3 demonstrate lower velocities. Specifically, particles along Path 3 ascend briefly under fluid forces before descending under the influence of gravity. Particles invading the clearances move slowly within the valve chamber and are fewer in number.

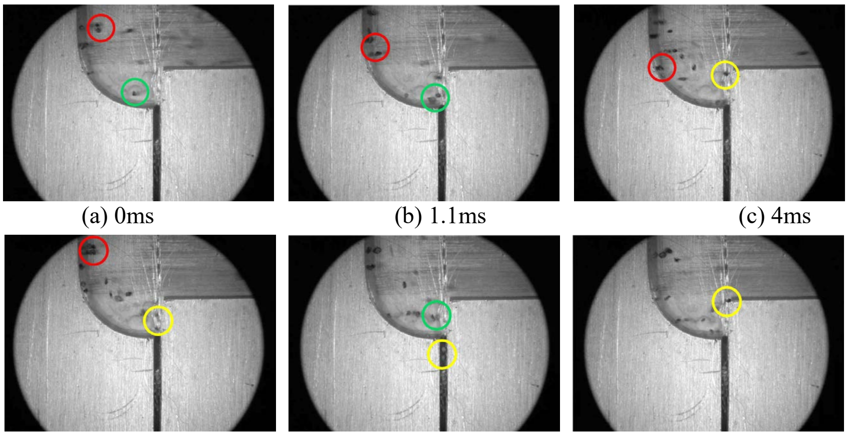

(a) 0ms (b) 1.1ms (c) 4ms

(d) 5.1ms (e) 6.2ms (f) 9.7ms

Figure 3.8. Particle Positions in the Lower Valve Chamber at Different Time Instants

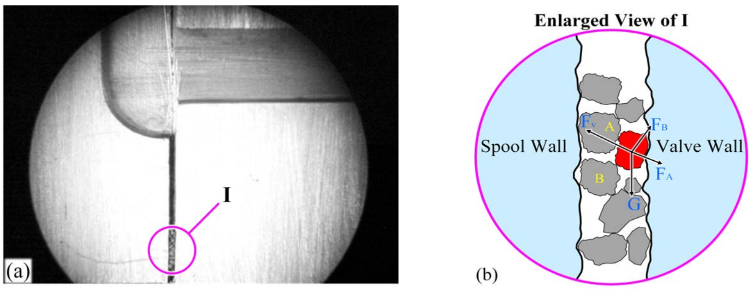

(a) Lower Valve Chamber and Clearance (b) Force Analysis on a Single Magnified Particle

Figure 3.9. Particle Retention After System Shutdown

Figure 3.8 illustrates particle positions in the lower valve chamber at sequential time instants. Observations reveal: Particles following Path 1 exhibit significantly higher velocities toward the outlet. Particles along Path 2 collide with the sleeve wall surface, subsequently descending to invade the lower clearance. Particles traversing Path 3 rebound upward upon collision with the sleeve wall, ultimately exiting along the wall surface.

Figure 3.9. illustrates the particle retention after shutting off the shut-off valve and system shutdown. Significant particle accumulation is observed in the lower clearance. This phenomenon arises because the interaction forces between aggregated particles, frictional forces exerted by the clearance walls, adhesive forces between particles and walls, and the gravitational force collectively cause the particles within the clearance to reach force equilibrium, thereby remaining trapped.

4. Valve Structural Optimization

4.1. Structural Design Variations

For the P-B operating condition, three distinct structural designs were developed: (1) Lowering the spool shoulder by 1.5 mm, (2) Aligning the spool shoulder flush with the outlet port, (3) Raising the spool shoulder by 1.75 mm. The geometric configurations of these designs are detailed in Table 1.

Table 1 Modified Spool Shoulder Models and Post-Modification Flow Trace Diagrams

Designation	Original Model	Lowering the Spool Shoulder	Spool Shoulder-Aligned	Raising the Spool Shoulder
Model Number	**O**	**I**	**II**	**III**
Geometric Model	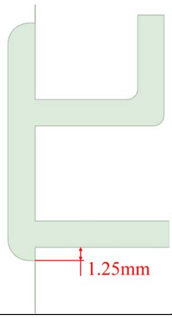	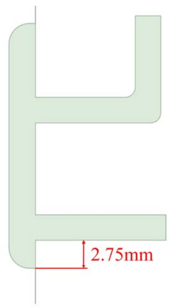	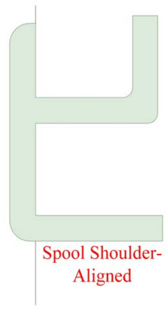	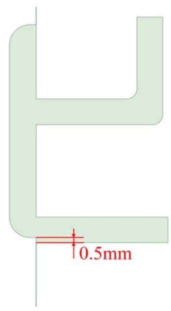
Flow Trace Diagrams	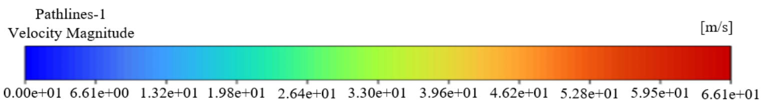 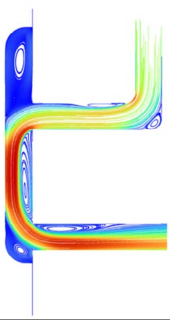	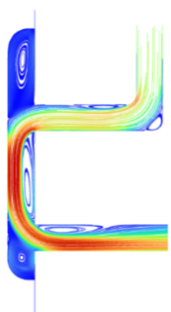	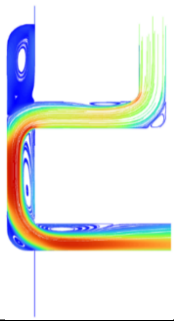	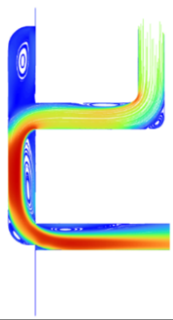

4.2. Simulation of Different Structures

A comparative simulation analysis was conducted for the three designs. Performance was evaluated based on particle retention rate and clearance invasion rate, leading to the identification of the optimal design. The flow trace diagrams for each structure are summarized in Table 1.

Structure I: 40 particles remained in the valve chamber at the end of the simulation. Total invasion rate: 44/600 = 7.3% (29 particles in the lower clearance (29/600 = 4.8%); 15 particles in the upper clearance (15/600 = 2.5%)).

Structure II: 92 particles were retained within the valve chamber at the end of the simulation. Total invasion rate: 7/600 = 1.2% (3 particles in the upper clearance (3/600 = 0.5%); 4 particles in the lower clearance (4/600 = 0.6%)).

Structure III: 24 particles remained in the valve chamber at simulation completion. Total invasion rate: 10/600 = 1.7%, with all invading particles exiting through the upper clearance outlet. Lower clearance invasion rate: 0/600 = 0% (no particles invaded). Upper clearance invasion rate: 16/600 = 2.6%.

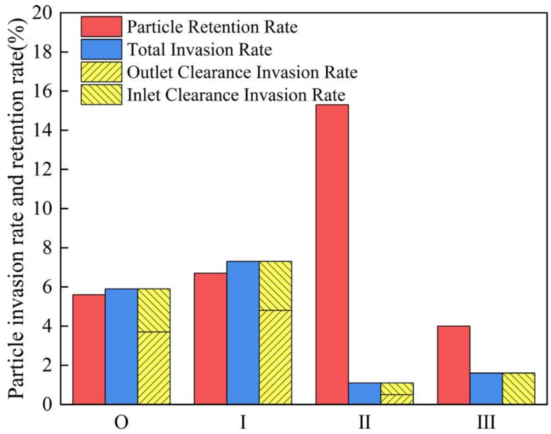

Figure 4.1. Particle Retention and Invasion Rates for Different Structural Models

Figure 4.1 illustrates the particle retention and invasion rates for different structural models. A comparative analysis of four models — the original model, spool shoulder-lowered model, spool shoulder-aligned model, and spool shoulder-raised mode — reveals the following:

- (1) Retention Rate Analysis: The spool shoulder-raised model reduced particle retention by 1.7% compared to the original model. The spool shoulder-lowered and spool shoulder-aligned models exhibited increased retention rates of 1.1% and 9.6%, respectively.
- (2) Invasion Rate Analysis: The spool shoulder-aligned and spool shoulder-raised models reduced invasion rates by 4.8% and 4.3%, respectively. Notably, the lower clearance invasion rate for the raised model was 0%. The spool shoulder-lowered model increased the invasion rate by 1.4%.

Conclusion: Considering both retention and invasion rates, the spool shoulder-raised model demonstrates optimal performance.

5. Conclusions

(1) Experimental results demonstrate that particles within the 0~5 μm, 0~10 μm, 0~20 μm, and 0~30 μm size ranges induce maximum stiction forces of 79.63 N, 127.7 N, 84.73 N, and 62.14 N, respectively, in the 5~10 μm clearance between the spool and sleeve. The 0~10 μm particles generated the highest stiction force, confirming that critical particles (sensitive particles) with sizes comparable to the spool clearance are the primary contributors to spool friction.

(2) Simulation analysis revealed particle migration and clearance invasion dynamics. At simulation completion, the retention rate in the valve chamber was 5.6%, with a total invasion rate of 5.8%. Smaller particles dominated invasion into the inlet-side clearance.

The vortex phenomenon significantly influenced particle trajectories, causing some particles to circulate within the chamber and eventually become trapped.

(3) Visualization experiments showed that most particles entering the valve chamber with the fluid were flushed out. A small fraction remained trapped in vortex-driven rotations near the outlet or invaded the upper/lower clearances. Post-shutdown, particles invading the clearances were not expelled by gravity but aggregated due to particle-wall interaction forces. Particles rotating in vortices settled at the chamber base after shutdown.

(4) Three spool shoulder optimizations were tested: lowering, aligning, and raising the shoulder. Simulations yielded retention rates of 6.7%, 15.3%, and 4%, and total invasion rates of 7.3%, 1.1%, and 1.6%, respectively. The spool shoulder-raised design demonstrated superior performance when balancing retention and invasion metrics.

6. REFERENCES

[1] M. A P R, A. C G R, R. L, et al. Water Microturbines for Sustainable Applications: Optimization Analysis and Experimental Validation[J]. Water Resources Management,2023, 38(3):1011-1025.

[2] Jia-yi W, Yang Y, Zhen-bo L, et al. Modal and structural analysis on a main feed water regulating valve under different loading conditions[J]. Annals of Nuclear Energy, 2021, 159.

[3] Jie D, Yipan D, Wenbin C, et al. Wear failure analysis of suction valve for high pressure and large flow water hydraulic plunger pump[J]. Engineering Failure Analysis, 2022, 134.

[4] Liang L, Peng Y X, Ru M L, et al. Analysis of fretting wear behavior of unloading valve of gasoline direct injection high pressure pump[J]. Journal of Zhejiang University-SCIENCE A, 2022, 23(4): 314-328.

[5] Hao T, Jianbo L, Yongjun G. Rapid diagnosis of proportional valve pilot stage stiction fault via dynamic model-based temporal features[J]. Proceedings of the Institution of Mechanical Engineers, 2025, 239(2): 373-388.

[6] Kazama T, Aoki S, Kobessho M. Cavitation Erosion Characteristics of High Bulk Modulus Oils: Preliminary Evaluation Experiment for Hydraulic Equipment[J]. Materials Performance and Characterization, 2020, 9(1): 20200003.

[7] Borivoj N, Ljiljana R, Mića Đ, et al. Analysis of the Behaviour of the Hydraulic Fluid HM VG 32 and HV 32 at Different Operating Conditions of the Axial-Piston Pump[J]. Tehnički vjesnik, 2024, 31(5): 1523-1529.

[8] Yang W, Li R, Xu J, et al. CFD-based axial steady-state hydrodynamic study and structural optimization of miniature switching valve[J]. Flow Measurement and Instrumentation, 2024, 100102744-102744.

[9] Li J, Peng C, Guo Q, et al. Study on Flow Field Characteristics of Micro-Flow Control Valve Based on Fluid-Thermal-Solid Coupling[J]. Arabian Journal for Science and Engineering,2024,50(12):1-18.

[10] Lin Z.H. Mechanisms of Spool Jamming in Hydraulic Valves and Mitigation Strategies [D]. Hangzhou: Zhejiang University; 2023. Dissertation Number: 2023.000863.

[11] Lin Z.H., Nie J.X., Hua T.F., et al. Solid-Liquid Flow Dynamics and Jamming in Hydraulic Spool Valves: A Clearance Analysis[J]. Chinese Hydraulics & Pneumatics, 2024, 48(3):115-120.

[12] Qian J, Xu J, Zhong F, et al. Solid-liquid flow characteristics and sticking-force

analysis of valve-core fitting clearance[J]. Journal of Zhejiang University-SCIENCE A, 2023, 24(12): 1096-1105.
[13] N. V B, V. E M, Cai C J. Mechanical Admixture Influence in the Working Fluid on Wear and Jamming of Spool Pairs from Aircraft Hydraulic Drives[J]. Journal of Friction and Wear, 2021, 41(6): 526-530.
[14] Bian L, Guo J, Pan J. Micromechanics analysis for thermal expansion coefficients of three-phase particle composites[J]. Archive of Applied Mechanics, 2019, 89(8): 1641-1654.
[15] Sajjadi H, Salmanzadeh M, Ahmadi G, et al.Lattice Boltzmann method and RANS approach for simulation of turbulent flows and particle transport and deposition[J]. Particuology, 2016, 3062-72.
[16] Liu X, Ji H, Min W, et al. Erosion behavior and influence of solid particles in hydraulic spool valve without notches[J]. Engineering Failure Analysis, 2020, 108104262-104262.
[17] Kharoua N, Alshehhi M, Khezzar L. Effects of fluid flow split on black powder distribution in pipe junctions[J]. Advanced Powder Technology, 2016, 27(1):42-52.
[18] Zhang J, Ji H, Zhao W, et al. Numerical Investigation of Micrometer-Sensitive Particle Intrusion in Hydraulic Valve Clearances and Its Impact on Valve Performance[J]. Processes, 2024, 12(5): 864.
[19] Qiang X L, Fei L, Hong J, et al. Particle erosion transient process visualization and influencing factors of the hydraulic servo spool valve orifice[J]. Flow Measurement and Instrumentation, 2023, 89.
[20] Xinqiang L, Hong J, Fei L, et al. Particle motion and erosion morphology of the spool orifice in an electro-hydraulic servo valve under a small opening[J]. Proceedings of the Institution of Mechanical Engineers, Part C: Journal of Mechanical Engineering Science, 2022, 236(6): 3160-3173.

Biographies

Chen Qianpeng received his Ph.D. degree from Lanzhou University of Technology, China in 2022. He is currently serving as an Associate Professor and Master's Supervisor in the Department of Fluid Transmission and Control, College of Energy and Power Engineering, Lanzhou University of Technology. He is a recipient of the "Hiwin" Outstanding Ph.D. Thesis Award from the Chinese Mechanical Engineering Society and has been awarded research funding from the China National Natural Science Fund. His long-term research focuses on precision measurement and high-reliability design of hydraulic components, hydraulic system applications, and the development of specialized machinery.